pH Dependence of Cyanide Binding to the Ferric Heme Domain of the Direct Oxygen Sensor from *Escherichia coli* and the Effect of Alkaline Denaturation[†]

Anil K. Bidwai, Esther Y. Ok, and James E. Erman*

Department of Chemistry and Biochemistry, Northern Illinois University, DeKalb, Illinois 60115

Received May 12, 2008; Revised Manuscript Received July 21, 2008

ABSTRACT: The spectrum of the ferric heme domain of the direct oxygen sensor protein from *Escherichia coli* (*Ec*DosH) has been measured between pH 3.0 and 12.6. *Ec*DosH undergoes acid denaturation with an apparent pK_a of 4.24 ± 0.05 and a Hill coefficient of 3.1 ± 0.6 and reversible alkaline denaturation with a pK_a of 9.86 ± 0.04 and a Hill coefficient of 1.1 ± 0.1. Cyanide binding to *Ec*DosH has been investigated between pH 4 and 11. The *Ec*DosH−cyanide complex is most stable at pH 9 with a K_D of 0.29 ± 0.06 μM. The kinetics of cyanide binding are monophasic between pH 4 and 8. At pH ≥8.5, the reaction is biphasic with the fast phase dependent upon the cyanide concentration and the slow phase independent of cyanide. The slow phase is attributed to conversion of denatured *Ec*DosH to the native state, with a pH-independent rate of 0.052 ± 0.006 s^{-1}. The apparent association rate constant for cyanide binding to *Ec*DosH increases from 3.6 ± 0.1 M^{-1} s^{-1} at pH 4 to 520 ± 20 M^{-1} s^{-1} at pH 11. The dissociation rate constant averages (8.6 ± 1.3) × 10^{-5} s^{-1} between pH 5 and 9, increasing to (1.4 ± 0.1) × 10^{-3} s^{-1} at pH 4 and (2.5 ± 0.1) × 10^{-3} s^{-1} at pH 12.2. The mechanism of cyanide binding is consistent with preferential binding of the cyanide anion to native *Ec*DosH. The reactions of imidazole and H_2O_2 with ferric *Ec*DosH were also investigated and show little reactivity.

Heme proteins perform a broad spectrum of functions such as oxygen storage and transport, electron transfer, and catalysis of biological oxidations utilizing either H_2O_2 or O_2. Recently, a new class of heme proteins that serve as biological sensors has emerged (*1*−*4*). Examples in this class include oxygen-sensing proteins such as FixL[1] and the direct oxygen sensor protein from *Escherichia coli* (*Ec*Dos), nitric oxide-sensing proteins such as soluble guanylate cyclase, and the carbon monoxide-sensing protein, CooA (*1*−*4*).

Heme-based sensors detect the presence of small diatomic ligands such as O_2, NO, or CO and initiate cellular responses to changes in the availability of the ligand. Almost all of the heme-based sensors contain two functional domains. The N-terminal heme domain is the sensor domain that binds the ligand, while the C-terminal domain is a catalytic domain that possesses catalytic or DNA binding activity. Association of ligand with or dissociation of ligand from the heme triggers conformational changes that are relayed to the catalytic domain to regulate function.

*Ec*Dos was identified from sequence homology with the PAS domain of FixL (*5*). *Ec*Dos has an N-terminal heme-binding PAS domain and a C-terminal phosphodiesterase catalytic domain, and initial studies suggested that its physiological function may be involved in the switch between aerobic and anaerobic metabolism. The optical absorption spectrum of *Ec*Dos indicates that both the reduced and oxidized forms of the heme are predominantly low-spin and hexacoordinate. Homology modeling using the sequence and structure of the PAS domain of *Bradyrhizobium japonicum* FixL suggests that the heme ligands in *Ec*Dos are His-77 and Met-95 (*6*). The heme-binding PAS domain of *Ec*Dos, *Ec*DosH, has been characterized by a number of spectroscopic techniques and by X-ray crystallography (*6*−*10*). The spectroscopic properties and the crystallographic structure confirm that the heme iron is coordinated to His-77 and Met-95 in the ferrous form of *Ec*DosH. However, various spectroscopic techniques, along with studies using Met-95 mutants, have produced different results for the oxidized, met form of *Ec*DosH. Magnetic circular dichroism studies in the near-infrared region were used to confirm histidine−methionine coordination in met-*Ec*DosH (*6*). However, optical absorption, resonance Raman, circular dichroism, and magnetic circular dichroism studies of met-*Ec*DosH and a number of Met-95 mutants suggest that Met-95 is not a heme ligand in the oxidized form of the protein (*7, 8*). The X-ray structure of crystalline ferric *Ec*DosH shows water or hydroxide ion bound to the heme iron at the sixth coordination site, most likely the hydroxide ion (*9*). The heme

[†] This work was supported in part by the National Institutes of Health through Grant R15 GM59740.

* To whom correspondence should be addressed. Phone: (815) 753-6867. Fax: (815) 753-4802. E-mail: jerman@niu.edu.

[1] Abbreviations: *Ec*Dos, *E. coli* direct oxygen sensor full-length sequence, including all domains; *Ec*DosH, heme domain of *Ec*Dos; PAS, acronym for the three proteins, Per, ARNT, and Sim, which in turn are abbreviations for the *Drosophila* period clock protein (Per), the aryl hydrocarbon nuclear transporter (ARNT), and the *Drosophilia* single-minded protein (Sim); FixL, protein encoded by the *fixL* gene in various *Rhizobium* species; GdHb, *Glycera dibranchiata* hemoglobin; IPTG, isopropyl β-thiogalactopyranoside; K_D^{spec}, equilibrium dissociation constant determined from spectrophotometric titrations; K_D^{kin}, equilibrium dissociation constant calculated from the ratio of the cyanide dissociation and association rate constants; CT, charge-transfer bands in the optical absorption spectrum; NIR, near-infrared. Site-specific mutations are specified by the one-letter codes for the amino acid residue in the wild-type protein followed by the primary sequence position and the one-letter code for the amino acid residue in the mutant; thus, M95A represents a mutant in which methionine at position 95 in the wild-type protein is replaced with alanine in the mutant.

10.1021/bi800872d CCC: $40.75
Published on Web 09/05/2008

environment in both the oxidized and reduced form of the protein is very hydrophobic with the heme surrounded by isoleucine, leucine, and valine residues.

Studies of the interaction of small molecules with heme proteins have often been useful in improving our understanding of structure−function relationships in heme proteins. Heme proteins bind small ligands in the ferrous and ferric states. Among the ferrous heme ligands, O_2, CO, and NO are important. Takahashi and Shimizu (*11*) have shown that the phophodiesterase activity of *Ec*Dos is significantly enhanced when either O_2 or CO binds to the ferrous form of the enzyme. Ferric heme ligands include cyanide, azide, fluoride, and imidazole. Rates of association and dissociation of these ligands as well as their affinities provide useful clues about the effect of heme environment on the chemical reactivity of different functional classes of heme proteins.

Watanabe and co-workers (*12*) have investigated cyanide binding to ferric *Ec*Dos and *Ec*DosH under limited conditions and report cyanide association rate constants of 2.2 M^{-1} s^{-1} for *Ec*Dos, 45 M^{-1} s^{-1} for *Ec*DosH, and 500 M^{-1} s^{-1} for the M95A mutant of *Ec*DosH at pH 7.5. Gonzalez et al. (*6*) found somewhat slower cyanide association rates for *Ec*DosH and its M95I mutant at pH 8, 14 and 71 M^{-1} s^{-1}, respectively. Watanabe et al. (*12*) also report very low affinities for azide, imidazole, and fluoride binding by *Ec*Dos and *Ec*DosH.

The binding of ligands such as cyanide, azide, fluoride, and imidazole to heme proteins is often pH-dependent due to protonation and/or deprotonation of the ligand as well as to weakly acidic or basic amino acid residues in the proximal and distal heme pockets (*13*−*23*). The pH dependence of the association and dissociation rate constants as well as the equilibrium binding constants indicates that heme proteins can discriminate between the protonated and unprotonated forms of ligands that bind to the Fe(III) heme. The general consensus in the literature is that metmyoglobin and other oxygen storage/transport proteins bind the anionic forms of the Fe(III) ligands while the heme enzymes such as the peroxidases and monooxygenases bind the neutral forms of the ligands. It is of interest to determine whether ligand binding to the heme sensors is similar to that of the oxygen transport/storage heme proteins, to the heme enzymes, or to neither of the two classical classes of heme proteins. In this study, we report an investigation of the pH dependence of cyanide binding to *Ec*DosH. We conclude that cyanide binding to ferric *Ec*DosH is strongly affected by the apolar nature of the heme pocket and that cyanide binding is distinct from cyanide binding to either metmyoglobin or the heme enzymes.

MATERIALS AND METHODS

*Cloning, Expression, and Purification of EcDosH. Ec*DosH comprises codons 1−147 of the *E. coli yddU* gene (*24*). *E. coli* genomic DNA was used as a template to amplify this gene fragment using standard PCR technology. Primers were designed to introduce an NdeI and an EcoRI restriction site at the 5′ and 3′ ends of the amplified fragment, respectively. The amplified gene fragment was ligated into an expression vector, pET-24b(+) (Novagen), which is a T7-based vector having kanamycin as a selectable marker. The recombinant pET-24b(+)/DosH plasmid was used to express *Ec*DosH in *E. coli*.

The pET-24b(+)/DosH plasmid was transformed into *E. coli* BL21(DE3), and a 1 L culture was grown at 37 °C in TB medium containing 20 μg/mL kanamycin. Expression was induced with 1 mM isopropyl β-thiogalactopyranoside (IPTG) at an OD_{600} of 1−1.2. The induced culture was grown overnight at 28 °C. Cells were harvested and lysed in a French press. The supernatant containing *Ec*DosH was applied to a Sephadex G-75 gel filtration column and eluted with a buffer containing 20 mM potassium phosphate and 100 mM NaCl (pH 7.5). Fractions containing the protein were pooled and applied to a DEAE-Sepharose (FastFlow) column and eluted with a 50 to 500 mM NaCl gradient over 300 mL. The purity of the protein was determined by SDS−PAGE and UV−vis spectroscopy. The purity index (ratio of absorbance at the Soret maximum to that at the maximum of the protein band near 276 nm) was generally between 2.7 and 3.0.

Buffers. All buffers used in this study have an ionic strength of 0.12 M and contain a minimum of 0.020 M KCl. Buffer compositions were as follows: pH 3.0−3.5, 0.010 M phthalate, 0.090 M KH_2PO_4, and KCl to adjust the ionic strength; pH 4.0−5.5, 0.010 M acetate, 0.090 M KH_2PO_4, and sufficient KCl to adjust the ionic strength; pH 5.5−8.0, 0.100 M in ionic strength from KH_2PO_4/K_2HPO_4 and 0.020 M KCl; pH 8.0−10.0, 0.100 M Tris-HCl with sufficient KCl to adjust the ionic strength; pH 9.0−11.0, 0.10 M glycine and sufficient KCl to adjust the ionic strength; pH 11.0−12.6, 0.100 M in ionic strength from K_2HPO_4/K_3PO_4 and 0.020 M KCl, with KOH added to adjust the pH above 11.5. Because of specific ion effects in the alkaline transition region, a second series of buffers containing only potassium phosphate salts and KCl was prepared between pH 6.0 and 12.6; the potassium phosphate salts contributed 0.100 M to the ionic strength, and the remaining 0.020 M came from KCl. The buffering capacity of these buffers was low between pH 8 and 10, and the pHs of the solutions were measured before and after each experiment when using these buffers.

Spectroscopy. A Varian/Cary model 3E double-beam UV−vis spectrophotometer or a Hewlett-Packard 8452A diode array spectrophotometer was used for optical absorption measurements. Spectra obtained on the Varian/Cary model 3E instrument were acquired at 1 nm resolution, while those obtained using the Hewlett-Packard instrument were obtained at 2 nm resolution. Band positions determined from maxima in the absorbance spectrum have uncertainties of 1−2 nm. Band positions for unresolved peaks, those appearing as shoulders or as minor inflections, were estimated using a peak-fitting program (PeakFit, version 4.12, SeaSolve Software, Inc., Framingham, MA). The unresolved band positions depend somewhat on peak shape, and the estimates of peak position have uncertainties of ∼5 nm.

Circular dichroism (CD) spectra were acquired on an AVIV model 215 CD spectrophotometer.

Protein and ligand solutions were buffered at the desired pH, and the ionic strength was kept constant at 0.12 M. All measurements were taken at 25 °C. The concentration of ferric *Ec*DosH was determined using an extinction coefficient of 124 mM^{-1} cm^{-1} at the Soret maximum (*5*).

Equilibrium Constant Determinations. Spectroscopic changes associated with the formation of the cyanide complex enabled monitoring of complex formation. Equi-

librium dissociation constants were determined via titration of 5−10 μM protein with increasing concentrations of cyanide. Separate samples were prepared for each different cyanide concentration and incubated overnight in capped tubes to ensure complete equilibration. The absorbance spectrum of each of the incubated solutions was determined, and the equilibrium dissociation constants were determined from plots of the change in absorbance, typically at 426 nm, versus cyanide concentration. Equilibrium studies were carried out at integral pH units between pH 5 and 11 at an ionic strength of 0.12 M and 25 °C.

Kinetic Measurements. Slow reactions, utilizing manual mixing, were monitored using the Hewlett-Packard 8452A diode array spectrophotometer. Rapid reactions were carried out using an Applied Photophysics Ltd. model DX.17MV stopped-flow instrument. All kinetic runs were conducted at 25 °C.

Cyanide binding reactions were carried out under pseudo-first-order conditions with excess cyanide. Observed rate constants were determined at a minimum of five different cyanide concentrations at each pH with the cyanide concentrations varying by a factor of at least 5 for each experiment. The total cyanide concentration varied between 1 and 50 mM depending on the pH. A minimum of 10 individual traces of absorbance change versus time were acquired at each cyanide concentration, allowing the mean value of the observed rate constant and its standard deviation to be determined. Association rate constants were determined from the slope of plots of the observed rate constant as a function of the total cyanide concentration. Kinetic studies of the association reaction were carried out at every half-pH between pH 4 and 11 at an ionic strength of 0.12 M.

Cyanide dissociation rates were determined by removal of free cyanide from an equilibrium mixture of *Ec*DosH and KCN using gel filtration, followed by monitoring the conversion of the *Ec*DosH−cyanide complex to free *Ec*DosH using the Hewlett-Packard 8452A diode array spectrophotometer. Kinetic runs were typically initiated within ~5 min of application of the *Ec*DosH−cyanide sample to the top of the Sephadex column. During the kinetic run, complete spectra were acquired every 10 min for up to 20 h. The pH of the sample was determined before and after completion of the kinetic run, and the reported pH values are the average of the two determinations.

RESULTS AND DISCUSSION

Spectroscopic Properties of Ferric EcDosH. The UV−visible spectrum of *Ec*DosH is shown between pH 5.0 and 11.8 in Figure 1. The spectra were acquired after equilibrium was achieved at each pH. Spectra between pH 5 and 9 are consistent with previously published spectra of the heme domain of *Ec*Dos (*5, 6, 8, 25*−*27*). The spectrum is invariant between pH 5 and 8.5 and is characteristic of a predominantly hexacoordinate, low-spin ferric heme protein. At pH 7.0, the Soret maximum occurs at 417 ± 1 nm, with maxima for the α, β, and δ bands observed at 562 ± 2, 530 ± 2, and 367 ± 2 nm, respectively (Table 1). In addition, there are two weak, unresolved charge-transfer bands that appear above 600 nm and two unresolved charge-transfer bands appearing between the β and Soret bands. The two long-wavelength charge-transfer bands are designated CT-1A and CT-1B, and

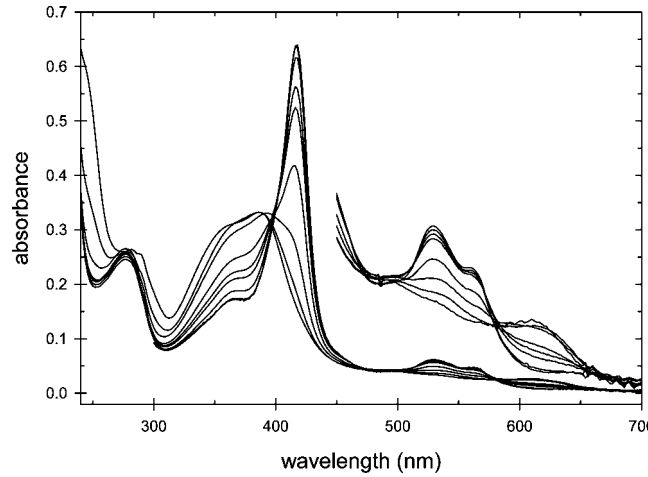

FIGURE 1: pH dependence of the absorption spectrum of *Ec*DosH. The spectrum of *Ec*DosH is independent of pH between pH 5 and 8.5 with the intensity of the Soret band decreasing above pH 8.5. Nine spectra are shown with those at pH 5.00 and 6.63 essentially identical and having the highest Soret intensity. The seven remaining spectra have decreasing absorbance at 418 nm in the following order: pH 8.70, 9.25, 9.40, 9.70, 10.24, 10.90, and 11.78. The visible region of the spectrum is shown magnified by a factor of 5. Experimental conditions: 5.15 μM *Ec*DosH, 0.12 M ionic strength buffers, 25 °C, data acquired with a Hewlett-Packard model 4352A diode array spectrophotometer. None of the spectra shown were acquired in buffers containing glycine.

Table 1: Spectroscopic Parameters for *Ec*DosH and Its Cyanide Complex at pH 7 and 11[a]

	λ (nm) [ε (mM^{-1} cm^{-1})]			
	*Ec*DosH		cyano*Ec*DosH	
	pH 7	pH 11	pH 7	pH 11
CT-1A	~706*sh* (0.9)	820 ± 20 (0.4)	−	−
CT-1B	~648*sh* (1.4)	~625*sh* (4.0)	−	−
α	562 ± 2 (9.0)	~587*sh* (4.4)	~568*sh* (8.5)	~568*sh* (8.9)
β	530 ± 2 (12)	~541*sh* (5.4)	540 ± 2 (11.1)	540 ± 2 (11.8)
CT-2A	~488*sh* (7.6)	~492*sh* (7.3)	~480*sh* (9.0)	~480*sh* (9.6)
CT-2B	~449*sh* (14)	−		
Soret (γ)	417 ± 1 (124)	390 ± 2 (51)	421 ± 1 (117)	421 ± 2 (119)
δ	367 ± 2 (36)	~351*sh* (44)	360 ± 2 (30)	360 ± 2 (31)

[a] Bands that appear as shoulders in the spectra are indicated by the designation *sh* immediately following the estimated peak position.

the two charge-transfer bands occurring between the β and Soret bands are designated CT-2A and CT-2B (Table 1). Figure 2 shows the visible and near-infrared region of the spectrum (450−900 nm) acquired using high concentrations of *Ec*DosH, which includes the two long-wavelength, charge-transfer bands CT-1A and CT-1B.

The observation of two charge-transfer bands above 600 nm suggests that ferric *Ec*DosH may be a mixture of two species with different heme ligation. The position of CT-1A, near 706 nm, is reminiscent of the 695 nm band in ferric cytochrome *c* (*28*) and provides some support for the notion that at least a fraction of ferric *Ec*DosH has histidine−methionine coordination in solution. Hydroxy-ligated methemoglobins and metmyoglobins typically have charge-transfer bands near 600 nm, while hydroxy-horseradish peroxidase has a CT band near 645 nm (*29*). The intensity and position of CT-1B in *Ec*DosH are similar to those of the charge-transfer band in hydroxy-ligated horseradish peroxidase. The crystal structure of ferric *Ec*DosH shows electron density

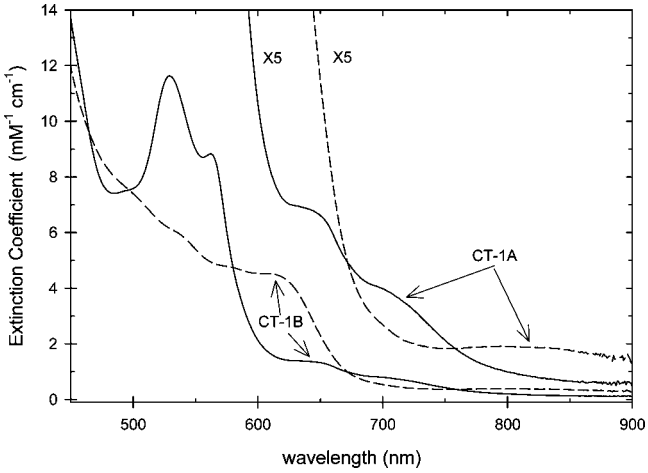

FIGURE 2: Visible and near-infrared (NIR) region of the spectrum of *Ec*DosH at pH 7.0 (—) and pH 11.6 (---). Between 600 and 900 nm, the spectra are also shown expanded by a factor of 5 to show the NIR charge-transfer band, CT-1A, at both pH values. The charge-transfer bands designated CT-1B are also labeled. Experimental conditions: 154 μM *Ec*DosH, 0.12 M ionic strength buffers, 25 °C, data acquired with a Varian/Cary model 3E spectrophotometer.

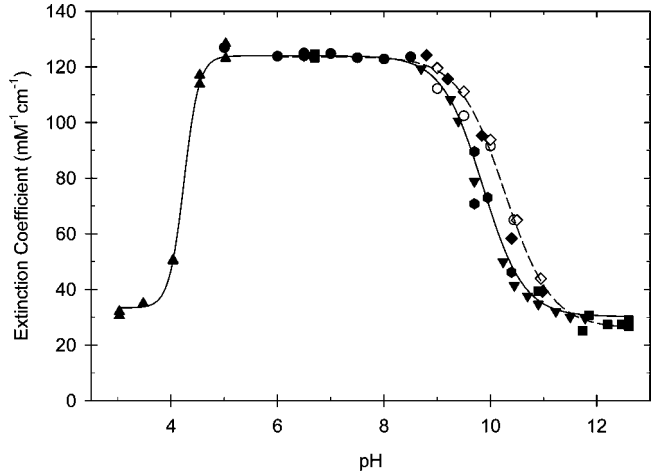

FIGURE 3: pH dependence of the extinction coefficient of *Ec*DosH at 418 nm. Filled symbols represent data acquired in buffers that do not contain glycine, while the empty symbols represent data obtained in buffers containing 0.10 M glycine. Different symbols indicate data acquired on different days, and two isolates of *Ec*DosH were used. The data were fit to an equation involving cooperative acid and alkaline transitions (eq 1). The apparent pK_a and Hill coefficient for the acidic transition are 4.24 ± 0.05 and 3.1 ± 0.6, respectively. In buffers that do not contain glycine, the apparent pK_a and Hill coefficient for the alkaline transition are 9.86 ± 0.04 and 1.1 ± 0.1, respectively. In 0.10 M glycine buffers, the apparent pK_a and Hill coefficient for the alkaline transition are 10.28 ± 0.03 and 1.0 ± 0.1, respectively. The best-fit values for the extinction coefficients at acidic, neutral, and alkaline pH are 34 ± 4, 124 ± 1, and 28 ± 2 mM^{-1} cm^{-1}, respectively. The lines shown in the figure were calculated using the best-fit parameters. Experimental conditions: 0.12 M ionic strength, 25 °C.

corresponding to a water molecule (or hydroxide ion) bound to the heme iron at the second axial position (*9*).

Spectroscopic data are most consistent with the binding of hydroxide rather than water, indicating that the heme-bound water has an abnormally low pK_a (<4). Whether the solution form of met-*Ec*DosH is a mixture of hydroxy-ligated and methionine-ligated hemes or has only hydroxide ion bound at the second axial position, the resonance Raman spectrum is invariant with respect to pH between pH 4 and 10 (*7*), and the optical absorption spectrum is invariant between pH 5 and 8.5 (Figure 1). The unusually low pK_a is a likely consequence of the very hydrophobic nature of the heme pocket in ferric *Ec*DosH (*9*) and the energy requirement to stabilize a water-ligated heme group in this pocket. The ferric heme has a net positive charge due to Fe(III) binding in the dianionic core of the heme group. Binding the negatively charged hydroxide ion neutralizes the core charge on the ferric iron, leading to a more stable heme complex within the hydrophobic heme pocket in *Ec*DosH.

pH Dependence of the Spectrum of EcDosH. One of the principle objectives of this study is to characterize the binding of cyanide to *Ec*DosH, especially to determine if *Ec*DosH discriminates between HCN and the cyanide anion. To do this, we must be able to investigate the cyanide binding reaction above pH 9 since the pK_a for the ionization of HCN is 9.04 under our experimental conditions (*30*). We have investigated the spectroscopic properties of *Ec*DosH over a wide pH range to establish the pH stability region for this protein. The spectrum of *Ec*DosH undergoes substantial changes at acid and alkaline pH as the protein denatures. Figure 1 shows the spectroscopic changes associated with alkaline denaturation, while spectra below pH 5 are shown in the Figure S1 of the Supporting Information. The absence of good isosbestic points in the spectra as the pH changes (Figure 1) suggests that the alkaline transition is complex. A plot of the extinction coefficient of *Ec*DosH at 418 nm between pH 3 and 12.6 is shown in Figure 3.

During investigation of the alkaline transition, it was noted that slightly different spectroscopic changes occurred in buffers containing 0.10 M glycine than in buffers that did not contain glycine, indicating that specific ions affected the alkaline transition (see Figure S2 of the Supporting Information). The data collected in glycine buffers are differentiated by the empty symbols in Figure 3. The cause of the specific ion effect is unknown but must be associated with differential binding of phosphate and glycine to *Ec*DosH. Glycine buffers stabilize the native form of *Ec*DosH relative to phosphate buffers, and the binding of at least one of these two ions must perturb the heme spectrum.

The extinction coefficient decreases sharply at low pH, indicating a highly cooperative pH-dependent transition, while the alkaline transition extends over a greater range of pH, whether in glycine or phosphate buffers. The pH dependence of the extinction coefficient at 418 nm was fit to eq 1 using nonlinear regression.

$$E = \frac{E_1\left(\frac{[H^+]}{K_{A1}}\right)^{n_1} + E_2 + E_3\left(\frac{K_{A2}}{[H^+]}\right)^{n_2}}{\left(\frac{[H^+]}{K_{A1}}\right)^{n_1} + 1 + \left(\frac{K_{A2}}{[H^+]}\right)^{n_2}} \quad (1)$$

Equation 1 allows for the possibility of cooperative pH-dependent transitions by including Hill coefficients, n_1 and n_2. The parameters E_1, E_2, and E_3 represent the limiting extinction coefficients under acidic, neutral, and alkaline conditions, respectively, while K_{A1} and K_{A2} are the apparent acid dissociation constants for the acidic and alkaline transitions, respectively. Best-fit values for E_1, E_2, and E_3 at 418 nm are 34 ± 4, 124 ± 1, and 28 ± 2 mM^{-1} cm^{-1}, respectively. In the acid region, pK_{A1} and n_1 are 4.24 ± 0.05

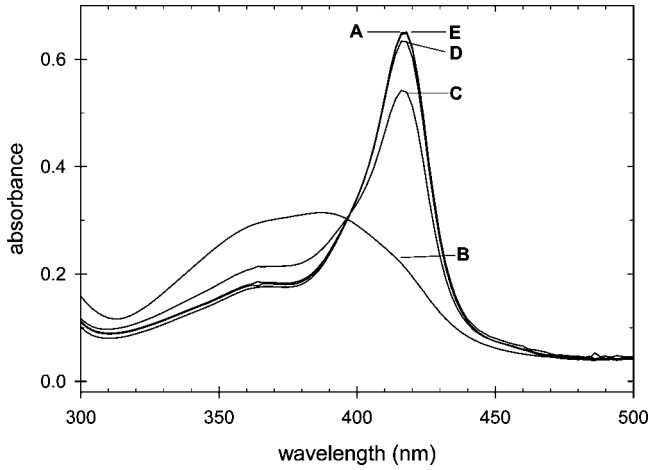

FIGURE 4: Reversibility of alkaline *Ec*DosH. (A) Spectrum of *Ec*DosH at pH 6.5, before exposure to alkaline pH. (B) Spectrum of *Ec*DosH after incubation of the sample for 5 min at pH 11.0. (C) Spectrum of *Ec*DosH immediately after the pH was reduced from 11.0 to 6.7. The spectrum was measure within 10 s of the pH change, and the sample has recovered 83% of its preincubation absorbance at the Soret maximum. (D) Spectrum of *Ec*DosH 5 min after the pH had been returned to 6.7. The absorbance at the Soret maximum is 97% of that of its preincubation value. (E) Spectrum of *Ec*DosH 80 min after the pH had been returned to 6.7. The sample has recovered 100% of its preincubation absorbance at the Soret maximum.

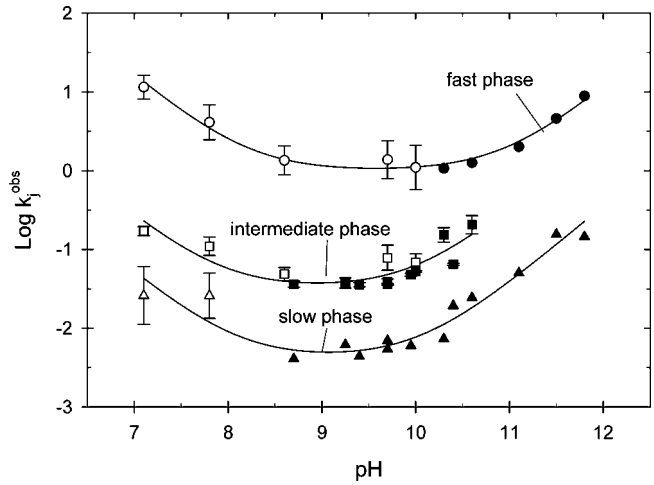

FIGURE 5: pH dependence of the three observed rate constants for the alkaline transition in *Ec*DosH. Filled symbols represent data obtained from forward pH jumps, while empty symbols represent data obtained from reverse pH jumps. The solid lines were calculated from eq 7 of the text and the best-fit parameters in Table 2.

and 3.1 ± 0.6, respectively. In the alkaline region, pK_{A2} and n_2 are 9.86 ± 0.04 and 1.1 ± 0.1, respectively, in phosphate buffers and 10.28 ± 0.03 and 1.0 ± 0.1, respectively, in glycine buffers. As one can see in Figure 3, the acid transition is highly cooperative with a Hill coefficient of 3.1 while the alkaline transition can be fit to a simple noncooperative transition. Glycine stabilizes the alkaline transition by 0.42 pH unit relative to phosphate.

Reversibility of the Alkaline Transition. The beginning of the alkaline denaturation of *Ec*DosH is evident at pH 9 (Figure 3), and this could interfere with the cyanide binding studies. Reversibility of alkaline denaturation would allow the cyanide binding studies to be extended to pH >9. The reversibility of the alkaline transition was investigated by incubating concentrated samples of *Ec*DosH at various alkaline pH values for 5 min followed by dilution with a concentrated pH 6.5 buffer and monitoring the spectrum of the protein at timed intervals following the return of the sample to neutral pH. Figure 4 illustrates a typical experiment, in this case incubating *Ec*DosH at pH 11 for 5 min before returning the sample to pH ~6.5. *Ec*DosH recovers 83% of its absorbance at the Soret maximum within the time it takes to manually mix the pH 11.0-incubated sample with pH 6.5 buffer and measure the spectrum, ~10 s. After a 5 min recovery period, the sample recovers 97% of the absorbance at 418 nm and 100% after 80 min. We conclude that the alkaline transition in *Ec*DosH is fully reversible when going from alkaline to neutral pH. Additional data demonstrating the reversibility of the alkaline transition are shown in Figure S3 of the Supporting Information.

Kinetics of the Alkaline Transition. We have investigated the kinetics of the alkaline transition in *Ec*DosH in both the forward and reverse direction. Up to three kinetic phases are observed during the alkaline transition, whether initiating the reaction by rapidly changing the pH of the sample from neutral to alkaline pH or vice versa, from alkaline pH to neutral pH. Both manual mixing and stopped-flow experiments were performed to monitor the reactions.

We define the observed rate constants as k_f^{obs}, k_i^{obs}, and k_s^{obs}, where the subscripts represent the fast, intermediate, and slow phases of the reaction, respectively. Plots of the logarithm of k_f^{obs}, k_i^{obs}, and k_s^{obs} for the alkaline transition as a function of pH are shown in Figure 5. The relative amplitudes of the kinetic phases as a function of pH are included in Figure S5 of the Supporting Information. The three kinetic processes indicate that a minimum of two intermediate forms of *Ec*DosH exist during the conversion of native *Ec*DosH to the final alkaline species.

A multicomponent, reversible reaction is difficult to analyze (*31, 32*). The alkaline transition involves at least four components, the native form, the denatured form, and at least two intermediates. A four-component, reversible system has six possible kinetic schemes, depending upon which components are directly converted to the others (*32*). The simplest scheme is the sequential mechanism shown in eq 2

Table 2: Best-Fit Values for the Coefficients Used To Define the Observed Rate Constants for the Three Kinetic Phases Observed during the Alkaline Transition in *Ec*DosH[a]

observed rate constant	C_{1j} (M^{-1} s^{-1})	C_{2j} (s^{-1})	C_{3j} (M s^{-1})
k_f^{obs}	$(1.6 \pm 0.2) \times 10^8$	0.99 ± 0.10	$(1.1 \pm 0.1) \times 10^{-11}$
k_i^{obs}	$(1.8 \pm 0.6) \times 10^6$	0.051 ± 0.011	$(3.9 \pm 1.1) \times 10^{-12}$
k_s^{obs}	$(4.9 \pm 1.8) \times 10^5$	$(4.1 \pm 1.0) \times 10^{-3}$	$(3.5 \pm 0.7) \times 10^{-13}$

[a] The observed rate constants and coefficients are defined in eq 7. The index *j* represents either f, i, or s for the fast, intermediate, or slow phase of the alkaline transition, respectively.

$$N \underset{k_{b1}}{\overset{k_{f1}}{\rightleftharpoons}} I_1 \underset{k_{b2}}{\overset{k_{f2}}{\rightleftharpoons}} I_2 \underset{k_{b3}}{\overset{k_{f3}}{\rightleftharpoons}} D \quad (2)$$

where N, I_1, I_2, and D represent the native form of *Ec*DosH, the two intermediate forms, and the denatured form, respectively. Six rate constants are required for this reaction mechanism, a forward rate constant, k_{fi}, and a back rate constant, k_{bi}, for each of the three steps, where the subscript *i* indicates the reaction step, either 1, 2, or 3. For this system of coupled, reversible reactions, each of the three observed rate constants is a complex function involving all six rate constants defined in eq 2, with the three observed rate constants given by the negative roots of a cubic equation (*31*). The three observed rate constants cannot be expressed in closed form, nor is there enough information to determine the values of the six rate constants defined in eq 2. The three observed rate constants are those of the normal reaction modes (*33, 34*) as the system re-equilibrates after a pH jump. We will treat the three observed rate constants phenomenologically.

pH Dependence of the Kinetics of the Alkaline Transition. Figure 5 includes the data for both forward (filled symbols) and reverse (empty symbols) pH jumps. We cannot detect the intermediate phase above pH 10.6, either because the rates of the fast and intermediate phases become too similar to deconvolute or because the amplitude of the intermediate reaction becomes too small to detect, or both. Between pH 11 and 12, the major decrease in absorption at 418 nm occurs during the fast phase of the reaction with the absorption actually increasing at 418 nm during the slowest phase of the reaction (see Figure S5 of the Supporting Information). This latter observation suggests that I_2 is a largely denatured form of *Ec*DosH.

All three observed rate constants are dependent upon pH, with minimum values occurring between pH 9 and 10 and increasing with increasing hydrogen or hydroxide ion concentrations. There are several ways to model the pH dependence of the observed rate constants. Since the alkaline transition has a Hill coefficient of 1 and essentially fits the titration of a single group (eq 1), we will model the alkaline transition by postulating that deprotonation of a single critical group triggers the alkaline transitions, a group with an apparent pK_a near 10. The scheme shown in eq 2 is expanded to include the protonation states of the critical group in all four protein species (eq 4). The expanded scheme also indicates that the second intermediate is a denatured form of the protein. The rate constants defined in eq 4 have a

$$\begin{array}{ccccccc} & & k_{f11} & & k_{f21} & & k_{f31} & \\ & HN & \rightleftharpoons & HI_1 & \rightleftharpoons & HD_1 & \rightleftharpoons & HD_2 \\ & & k_{b11} & & k_{b21} & & k_{b31} & \\ pK_N \downarrow\uparrow & & pK_{I1} \downarrow\uparrow & & pK_{D1} \downarrow\uparrow & & pK_{D2} \downarrow\uparrow & \\ & & k_{f12} & & k_{f22} & & k_{f32} & \\ & N & \rightleftharpoons & I_1 & \rightleftharpoons & D_1 & \rightleftharpoons & D_2 \\ & & k_{b12} & & k_{b22} & & k_{b32} & \end{array} \quad (3)$$

second index that distinguishes the forward and back reactions of the protonated and deprotonated states of the protein species. The acid dissociation constant of the critical group may have different values in each of the four protein species, and these are indicated by pK_N, pK_{I_1}, pK_{D_1}, and pK_{D_2}. When the critical group is protonated, the equilibria favor formation of HN, the stable native form of *Ec*DosH in the neutral-pH region. When the pH is increased such that the critical group is deprotonated, the equilibria favor the denatured forms of *Ec*DosH.

In terms of the mechanism shown in eq 4, the forward and backward rates for interconversion of the various protein species will be pH-dependent depending upon their state of protonation. The form of the pH-dependent rate constants is given in eqs 4 and 5.

$$k_{fj} = \frac{k_{fj1}\dfrac{[H^+]}{K_{Aj}} + k_{fj2}}{\dfrac{[H^+]}{K_{Aj}} + 1} \quad (4)$$

$$k_{bj} = \frac{k_{bj1}\dfrac{[H^+]}{K_{Aj+1}} + k_{bj2}}{\dfrac{[H^+]}{K_{Aj+1}} + 1} \quad (5)$$

The index *j* in eqs 4 and 5 can be 1, 2, or 3 depending upon the reaction step, and K_{Aj} and K_{Aj+1} are the appropriate acid dissociation constants that affect the various rates, i.e., K_N, K_{I_1}, K_{D_1}, and K_{D_2}. Equations 4 and 5 provide a template for defining a phenomenological form of the observed rate constants.

Since the reactions are reversible, the equilibration rates will involve forward and backward rate constants and the observed rate constants will have the form shown in eq 6

$$k_j = \frac{C_{1j}[H^+] + C_{2j} + \dfrac{C_{3j}}{[H^+]}}{\dfrac{[H^+]}{C_{4j}} + 1 + \dfrac{C_{5j}}{[H^+]}} \quad (6)$$

where the index *j* can be f, i, or s for the fast, intermediate, or slow phase of the alkaline transition, respectively. The coefficients C_{1j}, C_{2j}, and C_{3j} will be complex functions of the forward and reverse rate constants and the acid dissociation constants defined in eq 4, respectively, while C_{4j} and C_{5j} will be functions of the acid dissociation constants only. Since there is no indication of saturation of any of the observed rate constants at the extremes of pH (Figure 5), the terms involving C_{4j} and C_{5j} in the denominator of eq 6 must be negligible and eq 6 can be simplified to eq 7. Equation 7 is used to fit the pH dependence of the three phases of the alkaline transition using nonlinear least-squares regression.

$$k_j = C_{1j}[H^+] + C_{2j} + \frac{C_{3j}}{[H^+]} \quad (7)$$

The best-fit values for the three coefficients, C_{1j}, C_{2j}, and C_{3j}, are collected in Table 2. The solid lines in Figure 5 were calculated from eq 7 using the best-fit values for the coefficients. The slowest rate for the alkaline transition occurs at the minimum of k_s^{obs} (Figure 5). Differentiation of eq 7 with respect to $[H^+]$ indicates that the minimum rate occurs at pH 9.07 and that the half-time for the slowest phase of the reaction at pH 9.07 is 2.5 min.

Nature of the Alkaline-Denatured Form of EcDosH. The UV−visible spectrum of *Ec*DosH above pH 11 (Figure 1

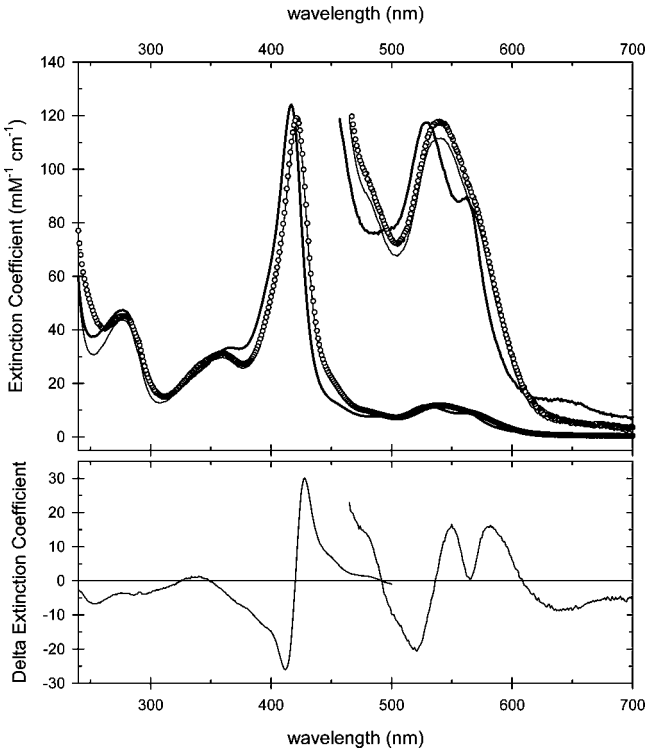

FIGURE 6: Spectra of *Ec*DosH and the *Ec*DosH−cyanide complex. The top panel shows the spectra of *Ec*DosH at pH 7 (thick solid line) and the *Ec*DosH−cyanide complex at pH 7 (thin solid line) and pH 11 (○). The visible region of the spectrum is shown with the vertical axis expanded by a factor of 10. The bottom panel shows the difference spectrum of the *Ec*DosH−cyanide complex minus that of *Ec*DosH at pH 7. The difference spectrum is multiplied by a factor of 10 above 480 nm.

and Supporting Information) is very similar to that of free heme in aqueous buffer (*35*), suggesting a largely unfolded protein with the heme exposed to solvent. However, circular dichroism studies indicate that the polypeptide chain retains elements of secondary structure in the alkaline form of *Ec*DosH (see Figure S6 of the Supporting Information), while the resonance Raman studies of Sato et al. (*7*) show that the heme group remains bound to the polypeptide chain up to at least pH 10, about halfway through the alkaline transition. We have additional evidence to support the conclusion that the heme remains bound to the polypeptide chain in the denatured forms of the protein and that the heme group in the alkaline-denatured form of *Ec*DosH has properties that are distinct from those of free heme (see Figure S7−S10 of the Supporting Information).

Equilibrium Binding Studies of Binding of Cyanide to EcDosH. Upon characterization of the alkaline transitions in *Ec*DosH, equilibrium studies on the binding of cyanide were initiated. The *Ec*DosH−cyanide complex is readily formed by adding buffered solutions of cyanide to the protein. The spectrum of the *Ec*DosH−cyanide complex at pH 7.0 is shown in Figure 6 along with that of the free protein. At pH 7.0, *Ec*DosH and the *Ec*DosH−cyanide complex have similar spectra since both have hexacoordinated low-spin heme groups. The Soret maximum of the cyanide complex is at 421 ± 1 nm, and the β band is at 540 ± 2 nm (Table 1). The α band becomes less distinct in the cyanide complex, appearing as a shoulder near 568 nm. The spectrum of the *Ec*DosH−cyanide complex is essentially independent of pH between pH 4 and 11. The spectrum of

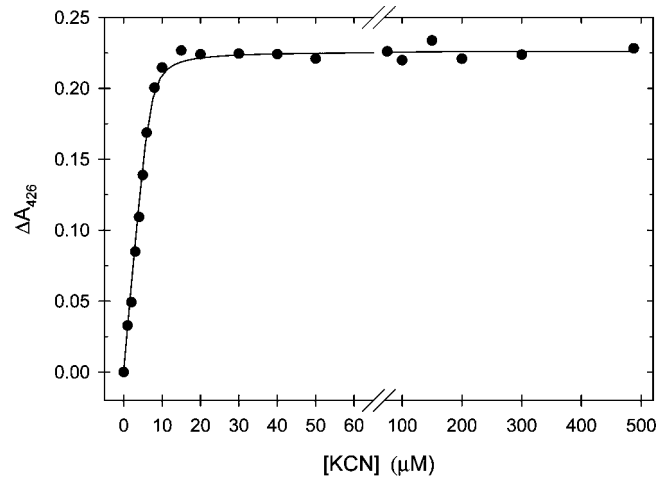

FIGURE 7: Absorbance change at 426 nm for *Ec*DosH upon overnight incubations in the presence of 0−500 μM buffered KCN. Conditions: 7.2 μM *Ec*DosH, pH 9.0, 0.12 M ionic strength, and 25 °C.

the *Ec*DosH−cyanide complex at pH 11 is shown in Figure 6 along with that of the complex at pH 7 for comparison. Spectroscopic parameters are listed in Table 1. The spectrum of the *Ec*DosH−cyanide complex at pH 11 provides additional evidence that the alkaline transition in *Ec*DosH is reversible since the spectrum of the cyanide complex with free heme at pH 11 is quite different from that of the *Ec*DosH−cyanide complex (Figure S11 of the Supporting Information).

The bottom panel of Figure 6 shows the difference spectrum between *Ec*DosH and its cyanide complex at pH 7.0. The largest absorption change occurs near 426−428 nm, and these wavelengths are generally used to monitor the binding of cyanide. A typical plot of the absorption change at 426 nm as a function of total cyanide concentration is shown in Figure 7 using data acquired at pH 9.0. The binding of cyanide is quite strong under the conditions of the experiment shown in Figure 7, and the absorbance change is a quadratic function of the total cyanide concentration (eq 8).

$$\Delta A_{obs} = \Delta A_{max} \frac{B - \sqrt{B^2 - 4PL}}{2P} \quad (8)$$

P and L represent the total protein and total cyanide concentrations, respectively, and B is equal to $P + L + K_D$. The data in Figure 7 were fit to eq 8 using nonlinear least-squares regression to extract best-fit values for the equilibrium dissociation constant, K_D. Values of K_D determined from the spectrophotometric titrations are designated K_D^{spec}. K_D^{spec} was determined at each integral pH between pH 5 and 11, and the data are collected in Table S2 of the Supporting Information. K_D^{spec} is pH-dependent, varying from 24 ± 4 μM at pH 5.0 to a minimum of 0.29 ± 0.06 μM at pH 9.0 (Figure 8). Above pH 9, in the alkaline transition region, the binding becomes weaker with K_D^{spec} increasing to 0.86 ± 0.13 μM at pH 11.

Rate of Binding of Cyanide to EcDosH. The binding of cyanide to *Ec*DosH is sufficiently fast that stopped-flow techniques were required to investigate the initial phases of the reaction. Typical traces of the change in absorbance at 426 nm are shown in Figure 9. The absorbance changes are

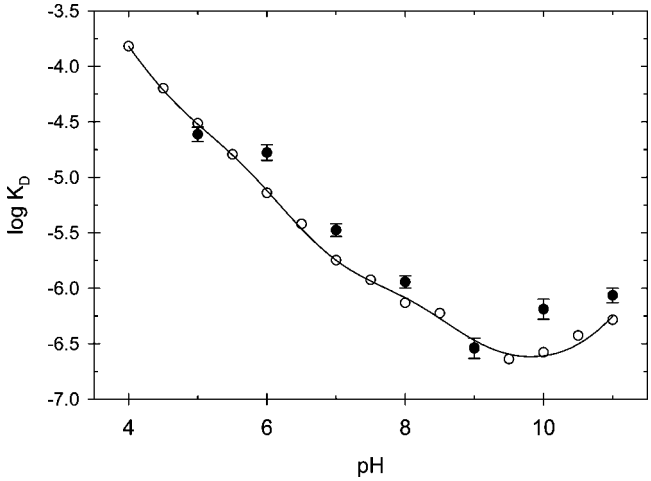

FIGURE 8: pH dependence of K_D^{spec} (●) and K_D^{kin} (○). The solid line was calculated using the ratio of dissociation (eq 12) and association (eq 11) rate constants and the best-fit parameters from Table 3.

Table 3: Kinetic Parameters for Cyanide Binding to *Ec*DosH[a]

parameter	value	parameter	value
k_1 (M^{-1} s^{-1})	3.5 ± 0.3	k_{-1}/K_{C1} (M^{-1} s^{-1})	4.6 ± 1.2
$k_2(K_L/K_{A3})$ + k_3 (M^{-1} s^{-1})	85 ± 13	k_{-2} + k_{-3} (s^{-1})	(8.9 ± 0.9) × 10^{-5}
k_4 (M^{-1} s^{-1})	470 ± 30	$k_{-4}K_{C2}$ (M s^{-1})	(1.7 ± 0.4) × 10^{-15}
pK_{A3}	6.9 ± 0.1	pK_{C1}	<4
pK_L	9.04[b]	pK_{C2}	>12

[a] Parameters are defined in eq 12. [b] The value of pK_L was fixed at the literature value for the HCN acid dissociation constant (*30*).

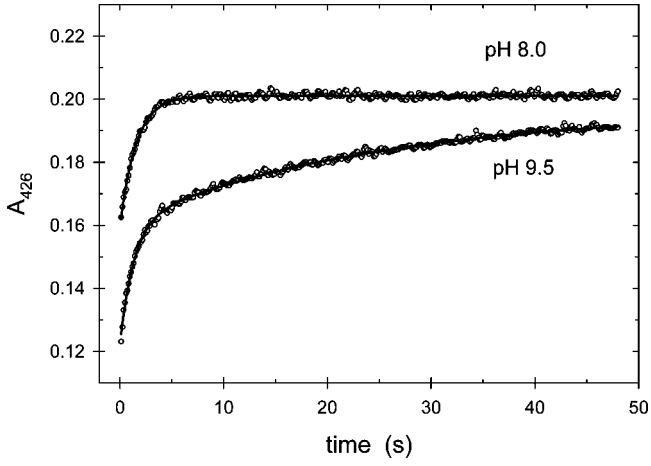

FIGURE 9: Time dependence of the absorbance change at 426 nm upon addition of buffered cyanide to *Ec*DosH at pH 8.0 and 9.5. Experimental conditions: 1.0 μM *Ec*DosH, 0.12 M ionic strength, 25 °C, 5 mM KCN at pH 8.0, 1 mM KCN at pH 9.5. The data at pH 8.0 fit a single-exponential function with an apparent rate constant of 0.64 ± 0.1 s^{-1}, while the data at pH 9.5 fit a double-exponential function with apparent rate constants of 0.76 ± 0.02 and 0.041 ± 0.001 s^{-1}.

monophasic between pH 4 and 8 and biphasic between pH 8.5 and 11. Between pH 4 and 8, the observed pseudo-first-order rate constant is designated k_{CN1} and is linearly dependent upon the cyanide concentration. Between pH 8.5 and 11, the faster of the two observed rate constants is linearly dependent upon the cyanide concentration and the equivalent of k_{CN1} at lower pH. The slower observed rate constant is independent of the cyanide concentration and

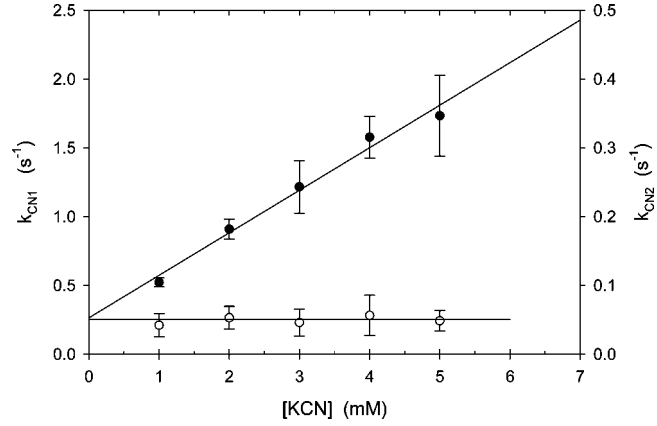

FIGURE 10: Plot of k_{CN1} (●, left-hand axis) and k_{CN2} (○, right-hand axis) as a function of KCN concentration at pH 9.0.

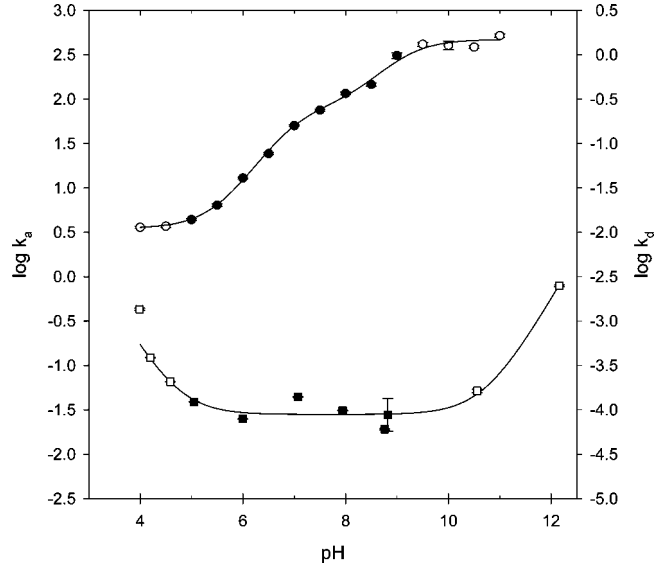

FIGURE 11: Plots of the logarithm of k_a (● and ○) and k_d (■ and □) as a function of pH. The filled symbols are for the data acquired between pH 5 and 9 where the absorbance of *Ec*DosH in independent of pH. The empty circles are for the data acquired at pH values where either acid or alkaline denaturation in *Ec*DosH occurs. The solid lines were calculated according to eqs 11 and 12 and the best-fit parameters listed in Table 3.

designated k_{CN2}. Representative plots of k_{CN1} and k_{CN2} as functions of the cyanide concentration are shown in Figure 10.

The apparent association rate constant for cyanide binding to *Ec*DosH, k_a, can be determined from the slope of plots of k_{CN1} as a function of the total cyanide concentration as shown in Figure 10. Values of k_a are collected in Table S3 of the Supporting Information. A plot of the logarithm k_a of as a function of pH is shown in Figure 11. The pH dependence of cyanide binding will be discussed below.

Slow Kinetic Phase in the Cyanide Binding Reaction. The slow, cyanide-independent phase of the cyanide binding reaction is observed between pH 8.5 and 11, within the alkaline transition region. The amplitude of this phase of the reaction correlates with the fraction of alkaline-denatured *Ec*DosH present in solution, increasing from zero at pH ~8 to a maximum of 77 ± 2% of the observed reaction at pH 10.5. The correlation breaks down at pH >11. The rate constants for the slow phase of the reaction, k_{CN2}, are collected in Table S3 of the Supporting Information. The

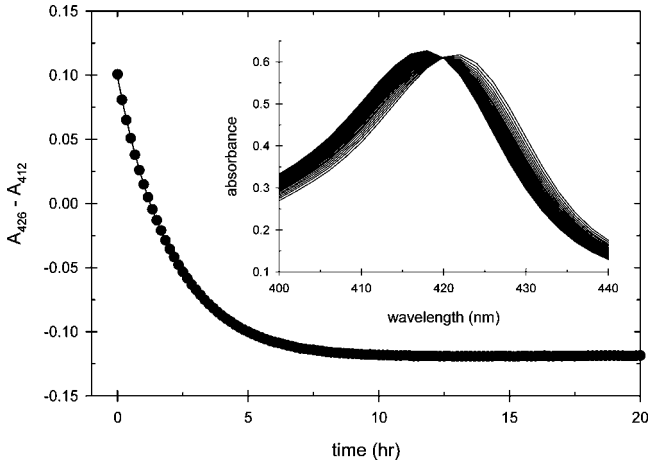

FIGURE 12: Dissociation of cyanide from the *Ec*DosH−CN complex at pH 5.05. The *Ec*DosH−CN complex was separated from free cyanide by being passed through a Sephadex G-10 column equilibrated in pH 5.05 buffer. Spectra of the separated *Ec*DosH−CN complex were acquired every 10 min for a period of 20 h using a diode array spectrophotometer. The first 60 spectra between 400 and 440 nm are shown in the inset. The magnitude of the *Ec*DosH−CN complex peak at 422 nm decreases, and that of the free *Ec*DosH peak at 416 nm increases with time. To correct for instrumental drift in the single-beam spectrophotometer, the difference in absorbance at 426 and 412 nm was calculated, and this difference is plotted as a function of time. The absorbances at 426 and 412 nm were chosen since these two wavelengths have large differences in absorbance between free *Ec*DosH and the *Ec*DosH−CN complex (see Figure 6). The difference in absorbance fits a single-exponential decay equation with a first-order rate constant of 0.48 ± 0.04 h^{-1}.

value of k_{CN2} is independent of pH between pH 8.5 and 11, with an average value of 0.052 ± 0.006 s^{-1}. This rate is similar to the intermediate phase of the alkaline transition, k_i^{obs} (Figure 5).

Rate of Dissociation of Cyanide from the EcDosH−CN Complex. The rate of dissociation of cyanide from the *Ec*DosH−CN complex is very slow, with a half-time on the order of hours in the neutral-pH region. The dissociation rate was measured by equilibrating *Ec*DosH and cyanide at pH 9, where the binding is strongest, and then removing unbound cyanide by gel filtration. The spectrum of the gel-separated *Ec*DosH−CN complex is monitored as a function of time as cyanide dissociates from the complex to reestablish equilibrium. Passage of the *Ec*DosH−cyanide sample through the gel filtration column also exchanges the buffer from pH 9 to a buffer of choice. The separated *Ec*DosH−CN complex equilibrates with the column buffer as it passes through the column, and the measured dissociation rate is that at the pH of the column buffer. The rate of cyanide dissociation was determined between pH 4 and 12 using this technique. A typical experiment is shown in Figure 12, where the dissociation rate is determined at pH 5. At pH 5, the half-time for dissociation of cyanide from the *Ec*DosH−CN complex is 1.4 ± 0.1 h, giving a dissociation rate constant, k_d, of (1.3 ± 0.1) × 10^{-4} s^{-1}. Values of k_d are collected in Table S3 of the Supporting Information, and a plot of the logarithm of k_d as a function of pH is shown in Figure 11.

Cyanide dissociation gives the native form of *Ec*DosH between pH ~4.5 and ~9. Below pH 4.5, the final product is acid-denatured *Ec*DosH, and above pH 11, the final product is alkaline-denatured *Ec*DosH. In Figure 11, when the product of cyanide dissociation is a predominantly denatured form of *Ec*DosH, the data are shown with empty symbols. An important observation is that the rate of cyanide dissociation is rate-limiting during formation of the denatured forms of *Ec*DosH from the *Ec*DosH−CN complex at both pH extremes. For example, the slowest phase of alkaline denaturation at pH 12 has a rate of 0.15 s^{-1}, while the rate of cyanide dissociation is ~2 orders of magnitude slower (2.5 × 10^{-3} s^{-1}). Likewise at pH 4.0, the rate of acid denaturation is 1.1 × 10^{-2} s^{-1}, ~1 order of magnitude faster than the rate of cyanide dissociation (1.4 × 10^{-3} s^{-1}).

An equilibrium dissociation constant for the *Ec*DosH−CN complex can be calculated from the ratio of dissociation and association rate constants. This kinetically determined equilibrium dissociation constant ($K_D^{kin} = k_d/k_a$) agrees quite well with K_D^{spec} (Table S2 of the Supporting Information and Figure 8). Between pH 5 and 9, where denaturation of *Ec*DosH is not a concern, the value of K_D^{kin} is on average 78% of that of K_D^{spec}. Above pH 9, the alkaline denaturation of *Ec*DosH influences K_D^{spec} and K_D^{kin} to different extents. The K_D^{kin} values reported in this work are ~7 times smaller (indicating stronger binding) than previously reported values calculated from the kinetic constants [9.1 μM at pH 7.5 (*12*) and 4.4 μM at pH 8.0 (*5, 6*)].

Mechanism of Cyanide Binding to EcDosH. Between pH 5 and 8, where the native form of *Ec*DosH is the dominant protein species in solution, cyanide binding appears to be a simple association reaction. At pH ≥8.5, a second reaction appears in the cyanide binding reaction, a reaction related to the rate of interconversion of protein species within the alkaline transition region. The slow reaction segregates the protein species into two groups, those that react rapidly with cyanide and those that do not react with cyanide. For the latter group, it is more favorable to isomerize to a reactive form of the protein than to react directly with cyanide itself. A basic mechanism for rationalizing binding of cyanide to *Ec*DosH is shown in eq 9 where $P_{reactive}$ represents the

$$\begin{array}{ccc} P_{reactive} + CN^- & \underset{k_d}{\overset{k_a}{\rightleftarrows}} & P{\cdot}CN \\ k_i \Updownarrow k_{-i} & & \\ P_{unreactive} & & \end{array} \qquad (9)$$

cyanide-reactive forms of *Ec*DosH and $P_{unreactive}$ represents the cyanide-unreactive forms of *Ec*DosH. Our current hypothesis is that $P_{reactive}$ includes the native and first intermediate forms of the protein observed in the alkaline transition (eqs 2 and 4), while the cyanide-unreactive forms are the two denatured forms of the protein, D_1 and D_2, in eq 4. In addition, we assume that the binding of cyanide to the native and first intermediate forms of *Ec*DosH is similar since we have no evidence to the contrary. The observed rate constant for conversion of the cyanide-unreactive forms to the cyanide reactive forms, k_{CN2}, is similar to the intermediate phase of the alkaline transition, k_i^{obs} (Figure 5).

An important observation is that some native *Ec*DosH exists in equilibrium with the denatured forms up to pH 11 and that the fast cyanide binding phase is the binding of cyanide to the native form of *Ec*DosH at all pH conditions. Thus, we can measure the association rate constant for cyanide binding to native *Ec*DosH between pH 4 and 11.

pH Dependence of Cyanide Binding to Native EcDosH. The pH dependence of the logarithm of k_a (Figure 11) shows two inflections, one near pH 7 and one near pH 9, indicating that a minimum of two ionizable groups influence the binding of cyanide to the reactive forms of *Ec*DosH. The inflection near pH 9 can be attributed to the acid dissociation constant of HCN, which has a pK_a of 9.04 at 25 °C, with an ionic strength of 0.12 M (*30*). The inflection near pH 7 has to be due to a group in *Ec*DosH that influences ligand binding but does not influence the spectroscopic properties of the protein (Figures 1 and 3).

A mechanism consistent with the pH dependence of both the association and dissociation rate constants for formation of the *Ec*DosH−cyanide complex is shown in eq 10. Two

$$\begin{array}{ccccc} & & & \overset{k_1}{\rightleftarrows} & \\ HN & + & HCN & \underset{k_{-1}}{} & H_2NCN \\ & pK_L & \updownarrow & & \updownarrow\ pK_{C1} \\ & & & \overset{k_2}{\rightleftarrows} & \\ HN & + & CN^- & \underset{k_{-2}}{} & HNCN \\ \updownarrow\ pK_{A3} & & & & \\ & & & \overset{k_3}{\rightleftarrows} & \\ N & + & HCN & \underset{k_{-3}}{} & HNCN \\ & pK_L & \updownarrow & & \updownarrow\ pK_{C2} \\ & & & \overset{k_4}{\rightleftarrows} & \\ N & + & CN^- & \underset{k_{-4}}{} & NCN \end{array} \qquad (10)$$

protonation states of the native form of *Ec*DosH, HN and N, are included in the mechanism shown in eq 10, related by an acid dissociation constant designated pK_{A3}. (Note that pK_{A1} and pK_{A2} were used to describe the acid and alkaline denaturations. It is possible that pK_{A3} in eq 10 is the same as pK_N in eq 4.) The mechanism shown in eq 10 allows for the binding of both HCN and the cyanide anion to both forms of the protein with unique rate constants. The acid dissociation constant for HCN is designated pK_L. Three different protonated forms of the complex must be included, and these are inter-related by two ionizations characterized by pK_{C1} and pK_{C2}. On the basis of the mechanism shown in eq 10, the pH dependence of the association rate constant is given by eq 11.

$$k_a = \frac{k_1 + \left(k_2\frac{K_L}{K_{A3}} + k_3\right)\frac{K_{A3}}{[H^+]} + k_4\frac{K_{A3}K_L}{[H^+]^2}}{\left(1 + \frac{K_{A3}}{[H^+]}\right)\left(1 + \frac{K_L}{[H^+]}\right)} \qquad (11)$$

The values of k_a were fit to eq 11 using nonlinear least-squares regression, and the best-fit values of the parameters are listed in Table 3. The solid line shown in Figure 11 was calculated using eq 11 and the parameters listed in Table 3.

The observation of the inflection near pH 9 in the plot of log k_a indicates that *Ec*DosH discriminates between the protonated and unprotonated forms of cyanide. When the pK_{A3} group is protonated at low pH, *Ec*DosH binds HCN with a bimolecular rate constant of 3.5 ± 0.3 M^{-1} s^{-1} (k_1 in eq 10 and Table 3). At high pH, when the pK_{A3} group is unprotonated, *Ec*DosH binds the cyanide anion with a rate constant of 470 ± 30 M^{-1} s^{-1} (k_4 in eq 10 and Table 3). At intermediate pH values, only upper limits can be established for k_2 and k_3. The upper limit for k_3, the binding of HCN to unprotonated *Ec*DosH, is 85 ± 13 M^{-1} s^{-1}, and the upper limit for k_2, the binding of the cyanide anion to the protonated form of *Ec*DosH, is 11000 ± 2000 M^{-1} s^{-1}. This analysis indicates that *Ec*DosH preferentially binds the cyanide anion rather than HCN since k_4 is larger than either k_1 or the upper limit for k_3. This contrasts with the binding of cyanide to such classic heme proteins as metmyoglobin and cytochrome *c* peroxidase, where HCN binds more rapidly than the cyanide anion (*15, 17*).

Another interesting observation concerning the pH dependence of the cyanide association rate constant is the apparent ionization near pH 7. The group with a pK_{A3} of 6.9 in *Ec*DosH is most likely in or near the heme pocket or possibly near the surface where cyanide enters the protein. Candidates for this group include a heme-bound water; His-77 (the proximal heme ligand), one of the two heme propionates, Asp-40 [part of the hydrogen bonding network in the proximal heme pocket (*6*)], and Arg-97, which stabilizes the bound oxygen in the oxyferrous form of the protein (*7*). A heme-bound water can be excluded from this list of potential candidates for the group with a pK_{A3} of 6.9 since the spectrum of *Ec*DosH is invariant with a pH between 5 and 8.5. There is ample evidence in the literature that the ionization of a heme-bound water will cause significant changes in the absorption spectrum (*29*), and this is not observed in *Ec*DosH. Asp-40 can also be excluded from the list since Watanabe et al. (*37*) have investigated cyanide binding to two Asp-40 mutants and have found only minor changes in the association rate constants at pH 7.5. Arg-97 is an intriguing candidate since it does interact with and stabilizes the heme-bound oxygen in the oxyferrous form of the protein (*10*). It is possible that, upon cyanide binding, Arg-97 could reorient and stabilize the cyanide complex just as it does the oxygen complex. We will have to wait for the crystal structure of the cyanide complex to see if this occurs. One problem with associating Arg-97 with the pK_{A3} 6.9 group is the low value of the pK_A. A pK_A of 6.9 is quite low for an arginine residue, although the pK_A of Arg-97 in unligated *Ec*DosH may be significantly perturbed due to interaction with two other charged groups, Arg-112 and Glu-98 (*10*).

The pH dependence of the cyanide dissociation rate constant is simpler than predicted by the mechanism shown in eq 10. Even though the data extend between pH 4 and 12, they do no extend far enough to determine the values of pK_{C1} and pK_{C2}. The most likely scenario is that pK_{C1} is less than 4 and pK_{C2} is greater than 12. The acid dissociation constant, K_{C1}, describes the dissociation of the proton from HCN as HCN binds to the heme iron in HP (eq 10). It is quite likely that the pK_A for HCN shifts from a value of 9 to a value of <4 upon cyanide binding to the heme iron. On the other hand, pK_{C2} refers to the dissociation of a proton from HCN as HCN binds to the P (eq 10). In this case, the proton could be transferred from HCN to the pK_{A3} group in the protein. If the proton is transferred from HCN to the pK_{A3} = 6.9 group, then pK_{A3} and pK_{C2} refer to dissociation of a proton from the same protein group, with the value of 6.9 in the free protein and a value of >12 in the protein−cyanide complex. Hydrogen bonding between the proton and the heme-bound cyanide could stabilize binding

of this proton and shift the pK_A from 6.9 to >12. Since pK_{C1} and pK_{C2} are outside of the range of study, the pH dependence of k_d based on the mechanism shown in eq 10 can be simplified to eq 12.

$$k_d = \frac{k_{-1}}{K_{C1}}[H^+] + (k_{-2} + k_{-3}) + \frac{k_{-4}K_{C2}}{[H^+]} \quad (12)$$

Fitting k_d as a function of pH provides best-fit values for three parameters, k_{-1}/K_{C1}, $k_{-2} + k_{-3}$, and $k_{-4}K_{C2}$. The best-fit values are collected in Table 3, and the solid line through the k_d data in Figure 11 is calculated from eq 12 using the values in Table 3. In the region where *Ec*DosH is stable, pH 5−9, k_d is independent of pH with a value of $(8.9 \pm 0.9) \times 10^{-5}$ s^{-1}. The rate of dissociation of cyanide from the *Ec*DosH−cyanide complex only increases in pH regions where the protein is denatured.

Comparison of Cyanide Binding in EcDosH and Other Heme Proteins. A survey of cyanide binding to heme proteins shows a remarkable diversity in the kinetics of the reaction near neutral pH (see Table S4 of the Supporting Information and references therein). The observed association rate constants vary by more than 9 orders of magnitude, from 2.25×10^{-3} M^{-1} s^{-1} for *Chromatium vinosum* cytochrome *c′* to 2.46×10^6 M^{-1} s^{-1} for spleen myeloperoxidase, while the observed dissociation rate constants vary by 7 orders of magnitude, from 1.4×10^{-6} s^{-1} for bovine cytochrome *c* oxidase to 22 s^{-1} for endothelial nitric oxide synthase. Studies of the pH dependence of cyanide binding indicate that heme proteins discriminate between HCN and the cyanide anion in their association reactions. The *c*-type cytochromes and some nonvertebrate hemoglobins preferentially react with the cyanide anion, while the peroxidases and mammalian metmyoglobins preferentially react with HCN.

Cyanide binding to metmyoglobin has been studied extensively, and its mechanism is most thoroughly understood (*38, 39*). At neutral pH, metmyoglobin is hexacoordinate with a water molecule bound to the sixth coordination site of the heme iron. A small amount of pentacoordinate metmyoglobin is in equilibrium with the hexacoordinate form. HCN diffuses into the heme pocket and is deprotonated to form the cyanide anion. The cyanide anion reacts rapidly with the pentacoordinate metmyoglobin to form the cyanide complex. The overall association rate will be influenced by diffusional partitioning of HCN into the heme pocket, the equilibrium between hexa- and pentacoordinate forms of metmyoglobin, and the rate of deprotonation of HCN in the heme pocket. Under the typical experimental conditions, deprotonation of HCN within the heme pocket is the rate-limiting step. Studies of metmyoglobin mutants (*38, 39*) suggest that deprotonation of HCN is affected by the polarity of the distal heme pocket and is facilitated to some extent through base catalysis by the distal histidine. Mutant studies suggest that small ligands enter the distal heme pocket through a polar channel gated by the distal histidine residue. Association rate constants for mammalian metmyoglobins near neutral pH are typically in the range of 100−500 M^{-1} s^{-1} and the dissociation rate constants $\sim 10^{-4}$ s^{-1}.

The peroxidases are pentacoordinate heme proteins and, as a class, react more rapidly with cyanide than any other class of heme proteins. The observed association rate constants at neutral pH are typically in the range 10^5−10^6 M^{-1} s^{-1} (see the Supporting Information). Just as with metmyoglobin, HCN diffuses into the distal heme pocket and deprotonation of the HCN appears to be the rate-limiting step. A distal histidine residue facilitates deprotonation of HCN by base catalysis, promoting the rate of association by at least 2 orders of magnitude (*17*). In cytochrome *c* peroxidase, replacement of the distal histidine with a leucine residue causes the mutant to react preferentially with the cyanide anion rather than HCN (*40*). The cyanide dissociation rate constants for the peroxidase are typically 0.1−5 s^{-1}. Although the observed rate constants for cyanide association and dissociation are both approximately 3−4 orders of magnitude faster for the peroxidases than for the mammalian metmyoglobins, the cyanide affinity is similar between these two classes of heme proteins.

Monomeric hemoglobins that lack a distal histidine residue such as those from *Glycera dibranchiata* (*41, 42*) react preferentially with the cyanide anion, presumably because there are no distal pocket residues to promote dissociation of a proton from HCN. The cyanide association rate constants are on the order of 0.3−2 M^{-1} s^{-1}, and the dissociation rate constants are also very slow, between 10^{-5} and 10^{-6} s^{-1}, resulting in cyanide affinities similar to those of the mammalian metmyoglobins and the peroxidases.

There are few studies on the pH dependence of cyanide binding to closed-crevice heme proteins such as the cytochromes. In one of the earliest studies, George and Tsou (*43*) found that horse cytochrome *c* reacted with both HCN and the cyanide anion. The cyanide anion reacted preferentially with a rate constant of 15 M^{-1} s^{-1}, while the HCN rate constant was 0.054 M^{-1} s^{-1}, ~300-fold slower. *C. vinosum* cytochrome *c′* is a pentacoordinate heme protein but has an active site that is so sterically hindered that the cyanide association rate constant is 2.25×10^{-3} M^{-1} s^{-1}, the slowest yet reported (*44*). *C. vinosum* ferricytochrome *c′* preferentially reacts with the cyanide anion, and the cyanide dissociation rate constant is 1.3×10^{-4} s^{-1}.

Studies of cyanide binding to the ferric states of heme sensor proteins, prior to this study, have been limited to experiments conducted at a single pH. Cyanide binding to full-length *Ec*Dos and to the isolated heme domains is slow, with association rate constants between 2.2 and 45 M^{-1} s^{-1} and dissociation constants varying from "too slow to measure" to 4.1×10^{-4} s^{-1} near pH 8 (*6, 12*). Reported association constants for full-length *Sm*FixL and the heme domain of *Sm*FixL and the heme domain of *Bj*FixL are similar to those of *Ec*Dos and range between 22 and 110 M^{-1} s^{-1} near pH 8, with dissociation rate constants varying from 1.0×10^{-4} to 4.7×10^{-4} s^{-1} (*45*−*47*).

The pH dependence of cyanide binding to *Ec*DosH (this study) is most similar to that of cytochrome *c* (*43, 44*) and the *G. dibranchiata* hemoglobin (GdHb) components II, III, and IV (*41, 42*) in that *Ec*DosH reacts preferentially with the cyanide anion. The pH-independent association rate constants for cyanide anion binding increase in the order 12, 15, 17, 73, and 470 M^{-1} s^{-1} for GdHb-III, cytochrome *c*, GdHb-II, GdHb-IV, and *Ec*DosH, respectively. For these proteins, HCN association rate constants can also be determined. The pH-independent HCN association rate constants are 0.52, 0.12, 0.22, 0.33, and 3.5 M^{-1} s^{-1} for cytochrome *c*, GdHb-III, GdHb-II, GdHb-IV, and *Ec*DosH, respectively. This group of heme proteins reacts between 30 and 220 times

faster with the cyanide anion than with HCN. The preference for the cyanide anion is most likely due to the difficulty in deprotonating HCN in the very nonpolar heme pockets of these proteins.

The binding of cyanide to representatives from the various classes of heme proteins displays distinct mechanisms associated with the structural properties of the heme pockets. While it is likely that HCN diffuses into the heme pockets more readily than the cyanide anion, those proteins that react preferentially with HCN require a mechanism for ionizing the HCN within the heme pocket. Both the peroxidases and the mammalian metmyoglobins contain distal histidines that can serve as base catalysts to promote internal HCN ionization, while the invertebrate hemoglobins, the cytochromes, and hemes sensor proteins lack such a residue. As a consequence, diffusion of the cyanide anion and direct binding of the cyanide anion to the positively charged heme iron in the very hydrophobic heme pocket make up the preferred mechanism for cyanide binding to *Ec*DosH and the other heme sensor proteins. Steric features and the polarity of the heme pockets in the various heme proteins cause differential diffusional barriers and differential partitioning between the solvent and the heme pocket for neutral and charged ligands such as HCN and CN^- and contribute to the determination of the absolute rates of cyanide binding to heme proteins (*9, 38, 39*).

Interaction of Imidazole and Hydrogen Peroxide with Ferric EcDosH. In addition to investigating the binding of cyanide to *Ec*DosH, we have also looked at two other typical reactions of ferric heme proteins, the binding of imidazole to the heme and the reaction of the heme with hydrogen peroxide. We do not detect any reaction between imidazole and *Ec*DosH using up to 1 M solutions of imidazole, consistent with a previous report (*12*). Likewise, *Ec*DosH does not react with hydrogen peroxide to form higher-oxidation state intermediates containing Fe(IV) as do the peroxidases or metmyoglobin. At high hydrogen peroxide concentrations, oxidative degradation of the heme is observed.

Comparison of Ligand Binding to Ferric and Ferrous EcDosH. Finally, it is interesting to compare the binding of the cyanide anion to ferric *Ec*DosH with the binding of neutral diatomic ligands to ferrous *Ec*DosH. The kinetics of ligand binding to both redox states of *Ec*DosH is slow compared to that of other heme proteins, suggesting a common feature is controlling the absolute ligand binding rates. The initial studies using the cloned PAS domain of *Ec*Dos, *Ec*DosH, reported association rate constants of 2.6×10^3, 1.1×10^3, and 1.8×10^3 M^{-1} s^{-1} for O_2, CO, and NO, respectively, at pH 7 (*5*). Taguchi et al. (*49*) reported somewhat faster rates for *Ec*DosH at pH 8 with association rate constants of 3.1×10^4 and 7.8×10^3 M^{-1} s^{-1} for O_2 and CO, respectively. Taguchi et al. (*49*) also reported association rate constants of 1.9×10^3 and 0.81×10^3 M^{-1} s^{-1} for O_2 and CO binding to full-length *Ec*Dos, respectively, at pH 8, ~10 times slower than to the isolated heme domain. O_2 and CO bind to ferrous *Ec*DosH with rates that are ~66 and ~17 times faster, respectively, than the rate of binding of the cyanide anion to ferric *Ec*DosH. These types of rate differences are reminiscent of the differential rates of diffusion of neutral and charged ligands into a variety of proteins (*50*).

SUPPORTING INFORMATION AVAILABLE

Figures showing spectra of *Ec*DosH at pH <5 and in glycine buffers at alkaline pH, experiments demonstrating the reversibility of the alkaline transition, circular dichroism spectra at pH 8 and 11, experiments demonstrating heme binding to the polypeptide chair at alkaline pH, values of the equilibrium and rate constants as a function of pH, and a survey of cyanide association and dissociation rate constants for 33 different heme proteins. This material is available free of charge via the Internet at http://pubs.acs.org.

REFERENCES

1. Sasakura, Y., Yoshimura-Suzuki, T., Kurokawa, H., and Shimizu, T. (2006) Structure-function relationships of *Ec*DOS, a heme-regulated phosphodiesterase from *Escherichia coli*. *Acc. Chem. Res. 39*, 37–43.
2. Chan, M. K. (2001) Recent advances in heme-protein sensors. *Curr. Opin. Chem. Biol. 5*, 216–222.
3. Rodgers, R. R. (1999) Heme-based sensors in biological systems. *Curr. Opin. Chem. Biol. 3*, 158–167.
4. Gilles-Gonzalez, M. A., Gonzalez, G., Perutz, M. F., Kiger, L., Marden, M. C., and Poyert, C. (1994) Heme based sensors, exemplified by the kinase FixL, are a new class of heme protein with distinctive ligand binding and autoxidation. *Biochemistry 33*, 8067–8073.
5. Delgado-Nixon, V. M., Gonzalez, G., and Gilles-Gonzalez, M. A. (2000) Dos, a heme-binding PAS protein from *Escherichia coli*, is a direct oxygen sensor. *Biochemistry 39*, 2685–2691.
6. Gonzalez, G., Dioum, E. H., Bertolucci, C. M., Tomita, T., Ikeda-Sato, M., Cheesman, M. R., Watmough, N. J., and Gilles-Gonzalez, M. A. (2002) Nature of the displaceable heme-axial residue in the *Ec*Dos protein, a heme-based sensor from *Escherichia coli*. *Biochemistry 41*, 8414–8421.
7. Sato, A., Sasakura, Y., Sugiyama, S., Sagami, I., Shumizu, T., Mizutani, Y., and Kitagawa, T. (2002) Stationary and time-resolved resonance Raman spectra of His^{77} and Met^{95} mutants of the isolated heme domain of a direct oxygen sensor from *Escherichia coli*. *J. Biol. Chem. 277*, 32560–32658.
8. Hirata, S., Matsui, T., Sasakura, Y., Sugiyama, S., Yoshimura, T., Sagami, I., and Shimizu, T. (2003) Characterization of Met95 mutants of a heme-regulated phosphodiesterase from *Escherichia coli*. Optical absorption, magnetic circular dichroism, circular dichroism, and redox potentials. *Eur. J. Biochem. 270*, 4771–4779.
9. Kurokawa, H., Lee, D., Watanabe, M., Sagami, I., Mikami, B., Raman, C. S., and Shimizu, T. (2004) A redox-controlled molecular switch revealed by the crystal structure of a bacterial heme PAS sensor. *J. Biol. Chem. 279*, 20186–20193.
10. Park, H., Suquet, C., Satterlee, J. D., and Kang, C. (2004) Insights into signal transduction involving PAS domain oxygen-sensing heme proteins from the x-ray crystal structure of *Escherichia coli* Dos heme domain (*Ec*DosH). *Biochemistry 43*, 2738–2746.
11. Takahashi, H., and Shimizu, T. (2006) Phosphodieterase activity of *Ec* DOS, a heme-regulated enzyme from *Escherichia coli*, toward 3′,5′-cyclic diguanylic acid is obviously enhanced by O_2 and CO binding. *Chem. Lett. 35*, 970–971.
12. Watanabe, M., Matsui, T., Sasakura, Y., Sagami, I., and Shimizu, T. (2002) Unusual cyanide binding to a heme-regulated phophodiesterase from *Escherichia coli*: Effect of Met95 mutations. *Biochem. Biophys. Res. Commun. 299*, 169–172.
13. Goldsack, D. E., Eberlein, W. S., and Alberty, R. A. (1965) Temperature jump studies of sperm whale metmyoglobin II. Azide and cyanate binding by metmyoglobin. *J. Biol. Chem. 240*, 4312–4315.
14. Goldsack, D. E., Eberlein, W. S., and Alberty, R. A. (1966) Temperature jump studies of sperm whale metmyoglobin III. Effect of heme-linked groups on ligand binding. *J. Biol. Chem. 241*, 2653–2660.
15. Ver Ploeg, D. A., Cordes, E. H., and Gurd, F. R. N. (1971) Comparison of myoglobins from harbor seal, porpoise, and sperm whale VII. Mechanism and catalysis for addition of cyanide to myoglobins. *J. Biol. Chem. 246*, 2725–2733.
16. Erman, J. E. (1974) Kinetic studies of fluoride binding by cytochrome *c* peroxidase. *Biochemistry 13*, 34–39.

17. Erman, J. E. (1974) Kinetic and equilibrium studies of cyanide binding by cytochrome *c* peroxidase. *Biochemistry 13*, 39–44.
18. Thanabal, V., DeRopp, J. S., and LaMar, G. N. (1988) Proton NMR characterization of the catalytically relevant proximal and distal hydrogen-bonding networks in ligated resting horseradish peroxidase. *J. Am. Chem. Soc. 110*, 3027–3035.
19. Merryweather, J., Summers, F., Vitello, L. B., and Erman, J. E. (1998) Metmyoglobin/fluoride: Effect of distal histidine protonation on the association and dissociation rate constants. *Arch. Biochem. Biophys. 358*, 359–368.
20. Lin, J., Merryweather, J., Vitello, L. B., and Erman, J. E. (1999) Metmyoglobin/azide: The effect of heme-linked ionizations on the rate of complex formation. *Arch. Biochem. Biophys. 362*, 148–158.
21. Taylor, K. C., Vitello, L. B., and Erman, J. E. (2000) 4-Nitroimidazole binding to horse metmyoglobin: Evidence for preferential anion binding. *Arch. Biochem. Biophys. 382*, 284–295.
22. Bidwai, A., Witt, M., Foshay, M., Vitello, L. B., Satterlee, J. D., and Erman, J. E. (2003) Cyanide binding to cytochrome *c* peroxidase (H52L). *Biochemistry 42*, 10764–10771.
23. Jacobson, T., Williamson, J., Wasilewski, A., Vitello, L. B., and Erman, J. E. (2004) Azide binding to yeast cytochrome *c* peroxidase and horse metmyoglobin: Comparative thermodynamic investigation using isothermal titration calorimetry. *Arch. Biochem. Biophys. 422*, 125–136.
24. Blattner, F. R., Plunkett, G., III, Bloch, C. A., Perna, N. T., Burland, V., Riley, M., Collado-Vides, J., Glasner, J. D., Rode, C. K., Mayher, G. F., Gregor, J., Davis, N. W., Kirkpatrick, H. A., Goeden, M. A., Rose, D. J., Mau, B., and Shao, Y. (1997) The complete genome sequence of *Escherichia coli* K-12. *Science 277*, 1453–1474.
25. Sasakura, Y., Hirata, S., Sugiyama, S., Suzuki, S., Taguchi, S., Watanabe, M., Matsui, T., Sagami, I., and Shimizu, T. (2002) Characterization of a direct oxygen sensor heme protein from *Escherichia coli.* Effects of the heme redox states and mutations at the heme-binding site on catalysis and structure. *J. Biol. Chem. 277*, 23821–23827.
26. Yoshimura, T., Sagami, I., Sasakura, Y., and Shimizu, T. (2003) Relationships between heme incorporation, tetramer formation, and catalysis of a heme-regulated phosphodiesterase from *Escherichia coli.* A study of deletion and site-directed mutants. *J. Biol. Chem. 278*, 53105–53111.
27. Suquet, C., Savenkova, M., and Satterlee, J. D. (2005) Recombinant PAS-heme domains of oxygen sensing proteins: High level production and physical characterization. *Protein Expression Purif. 42*, 182–193.
28. Dragomir, I., Hagarman, A., Wallace, C., and Schweitzer-Stenner, R. (2007) Optical band splitting and electronic perturbations of the heme chromophore in cytochrome *c* at room temperature probed by visible electronic circular dichroism spectroscopy. *Biophys. J. 92*, 989–998.
29. Vitello, L. B., Erman, J. E., Miller, M. A., Mauro, J. M., and Kraut, J. (1992) Effect of Asp-235 → Asn substitution on the absorption spectrum and hydrogen peroxide reactivity of cytochrome *c* peroxidase. *Biochemistry 31*, 11524–11535.
30. Izatt, R. M., Christensen, J. J., Pack, R. T., and Bench, R. (1962) Thermodynamics of metal-cyanide coördination. I. pK, $\Delta H°$, and $\Delta S°$ values as a function of temperature for hydrocyanic acid dissociation in aqueous solution. *Inorg. Chem. 1*, 828–831.
31. Rodiguin, N. M., and Rodiguina, E. N. (1964) *Consecutive Chemical Reactions: Mathematical Analysis and Development*, Van Nostrand Co., New York.
32. McLaughlin, E., and Rozett, R. W. (1971) Kinetics of complex systems tending to equilibrium. *Chem. Tech.,* 120–121.
33. Hammes, G. G., and Schimmel, P. R. (1970) Rapid Reactions and Transient States. In *The Enzymes, Vol. II, Kinetics and Mechanism* (Boyer, P. D., Ed.) 3rd ed., pp 67−114, Academic Press, New York.
34. Eigen, M., and De Maeyer, L. (1974) Theoretical Basis of Relaxation Spectrometry. In *Techniques of Chemistry, Volume VI, Investigation of Rates and Mechanisms of Reactions, Part II: Investigation of Elementary Reaction Steps in Solution and Very Fast Reactions* (Hammes, G. G., Ed.) 3rd ed., pp 64−146, Wiley-Interscience, New York.
35. De Villiers, K. A., Kaschula, C. H., Egan, T. J., and Marques, H. M. (2007) Speciation and structure of ferriprotoporphyrin IX in aqueous solution: Spectroscopic and diffusion measurements demonstrate dimerization, but not μ-oxo dimer formation. *J. Biol. Inorg. Chem. 12*, 101–117.
36. Deleted in press.
37. Watanabe, M., Kurokawa, H., Yoshimura-Suzuki, T., Sagami, I., and Shimizu, T. (2004) Critical roles of Asp40 at the haem proximal side of haem-regulated phosphodiesterase from *Escherichia* coli in redox potential, auto-oxidation and catalytic control. *Eur. J. Biochem. 271*, 3937–3942.
38. Brancaccio, A., Cutruzzolá, F., Allocatelli, T., Brunori, M., Smerdon, S. J., Wilkinson, A. J., Dou, Y., Keenan, D., Ikeda-Saito, M., Brantly, R. E., Jr., and Olson, J. S. (1994) Structural factors governing azide and cyanide binding to mammalian metmyoglobins. *J. Biol. Chem. 269*, 13843–13853.
39. Dou, Y., Olson, J. S., Wilkinson, A. J., and Ikeda-Saito, M. (1996) Mechanism of hydrogen cyanide binding to myoglobin. *Biochemistry 35*, 7107–7113.
40. Bidwai, A., Witt, M., Foshay, M., Vitello, L. B., Satterlee, J. D., and Erman, J. E. (2003) Cyanide binding to cytochrome *c* peroxidase (H52L). *Biochemistry 42*, 10764–10771.
41. Mintorovitch, J., and Satterlee, J. D. (1988) Anomalously slow cyanide binding to *Glycera dibranchiata* monomer methemoglobin component II: Implication for the equilibrium constant. *Biochemistry 27*, 8045–8050.
42. Mintorovitch, J., van Pelt, D., and Satterlee, J. D. (1989) Kinetic study of the slow cyanide binding to *Glycera dibranchiata* monomer hemoglobin components III and IV. *Biochemistry 28*, 6099–6104.
43. George, P., and Tsou, C. L. (1952) Reaction between hydrocyanic acid, cyanide ion and ferricytochrome c. *Biochem. J. 50*, 440–448.
44. Motie, M., Kassner, R. J., Meyer, T. E., and Cusanovich, M. A. (1990) Kinetics of cyanide binding to *Chromatium vinosum* ferricytochrome *c′*. *Biochemistry 29*, 1932–1936.
45. Rodgers, K. R., Lukat-Rodgers, G. S., and Barron, J. A. (1996) Structural basis for ligand discrimination and response initiation in the heme-based oxygen sensor FixL. *Biochemistry 35*, 9539–9548.
46. Winkler, W. C., Gonzalez, G., Wittenberg, J. B., Hille, R., Dakappagari, N., Jacob, A., Gonzalez, L. A., and Gilles-Gonzalez, M. A. (1996) Nonsteric factors dominate binding of nitric oxide, azide, imidazole, cyanide, and fluoride to rhizobial heme-based oxygen sensor FixL. *Chem. Biol. 3*, 841–850.
47. Dunham, C. M., Diouum, E. M., Tuckerman, J. R., Gonzalez, G., Scott, W. G., and Gilles-Gonzalez, M. A. (2003) A distal arginine in oxygen-sensing heme-PAS domains is essential to ligand binding, signal transduction, and structure. *Biochemistry 42*, 7701–7708.
48. Boffi, A., Ilari, A., Spagnuolo, C., and Chiancone, E. (1996) Unusual affinity of cyanide for ferrous and ferric *Scapharca inaequivalvis* homodimeric hemoglobin. Equilibria and kinetics of the reaction. *Biochemistry 35*, 8068–8074.
49. Taguchi, S., Matsui, T., Igarashi, J., Sasakura, Y., Araki, Y., Ito, O., Sugiyama, S., Sagami, I., and Shimizu, T. (2004) Binding of oxygen and carbon monoxide to a heme-regulated phophodiesterase from *Escherichia coli*. *J. Biol. Chem. 279*, 3340–3347.
50. Lakowicz, J. R., and Weber, G. (1973) Quenching of protein fluorescence by oxygen. Detection of structural fluctuations in protein on the nanosecond time scale. *Biochemistry 12*, 4171–4179.

BI800872D